Geophysical Research Letters

RE SEARCH LETTER
10.1029/2019GL084329

Testing for Dynamical Dependence: Application to the Surface Mass Balance Over Antarctica

Stéphane Vannitsem[1], Quentin Dalaiden[2], and Hugues Goosse[2]

[1]Royal Meteorological Institute of Belgium, Brussels, Belgium, [2]Earth and Life Institute, Université Catholique de Louvain, Louvain-La-Neuve, Belgium

Abstract Dynamical dependence between key observables and the surface mass balance (SMB) over Antarctica is analyzed in two historical runs performed with the MPI-ESM-P and the CESM1-CAM5 climate models. The approach used is a novel method allowing for evaluating the rate of information transfer between observables that goes beyond the classical correlation analysis and allows for directional characterization of dependence. It reveals that a large proportion of significant correlations do not lead to dependence. In addition, three coherent results concerning the dependence of SMB emerge from the analysis of both models: (i) The SMB over the Antarctic Plateau is mostly influenced by the surface temperature and sea ice concentration and not by large-scale circulation changes; (ii) the SMB of the Weddell Sea and the Dronning Maud Land coasts are not influenced significantly by the surface temperature; and (iii) the Weddell Sea coast is not significantly influenced by the sea ice concentration.

Key Points:
- The analysis of the rate of information transfer allows for clarifying dynamical dependence beyond the classical correlation analysis
- The surface mass balance over the Plateau, the central part of Antarctica, is mainly influenced by temperature and sea ice concentration
- The surface mass balance on the Weddell sea and Dronning Maud Land coasts displays a dynamics with a large influence of global-scale modes

Supporting Information:
- Supporting Information S1

Correspondence to:
S. Vannitsem,
svn@meteo.be

Citation:
Vannitsem, S., Dalaiden, Q., & Goosse, H. (2019). Testing for dynamical dependence: Application to the surface mass balance over Antarctica. *Geophysical Research Letters*, *46*, 12,125–12,135. https://doi.org/10.1029/2019GL084329

Received 28 JUN 2019
Accepted 26 SEP 2019
Accepted article online 16 OCT 2019
Published online 14 NOV 2019

1. Introduction

In the climatological literature, one often reads terminologies like *impact*, *driving mechanisms*, *influence*, *relationship*, *dependence*, and *coupling*, among many others, but the actual meaning of these terms are usually quite loose. These connections are often derived from a detailed analysis of the covariances or lag covariances between different observables. For instance, it is very often claimed that the El Niño-Southern Oscillation has an influence over many regions of the globe due to the strong teleconnections (covariances or lagged covariances) between the observables of the Tropical Pacific and other regions of the globe (Alexander et al., 2002; Brönnimann, 2007; Lau, 2016). Far from claiming that such (tele)connections do not exist, the statistical tools which are applied are however not appropriate to detect causal relationship if they are not complemented with additional analyses, such as sensitivity experiments with climate models for instance. Consequently, the terminology is used in a very loose sense, and conclusions can be difficult to draw.

The climate system and its components are dynamical systems whose descriptions are based on nonlinear dynamical equations, forced by both deterministic and random forcings. The way its different components and variables interact is complicated and can lead to intricate relations. How to disentangle the influence of one observable on another is an immense challenge, in particular when investigating sets of observations. Recent advances in dynamical system theories can considerably help in disentangling the influence of one observable on another. One particular approach developed by Sugihara et al. (2012) based on analog techniques in a reconstructed phase space has numerous potential applications (e.g., Luo et al., 2015; Tsonis et al., 2015; Vannitsem & Ekelmans, 2018; Ye et al., 2015, Ma et al., 2018), see also Vannitsem and Ghil (2017) for an other analog-based approach. One drawback is the necessity to define an appropriate phase space to reconstruct the attractor of the system.

Another methodology is based on the flow of information, derived from the notion of information entropy introduced originally by Shannon (1948). This approach has been advocated for many years (e.g., Abarbanel et al., 2001; Bianco-Martinez & Baptista, 2018; Deza et al., 2015; Hlavackova-Schindler et al., 2007; Krakovská et al., 2018; Liang & Kleeman, 2005; Runge et al., 2012; Schreiber, 2000; Vastano & Swinney, 1988). In this framework, a rigorous formalism for the transfer of information from one set of variables of a dynamical system to another has been recently put forward (Liang & Kleeman, 2005; 2007). Since then, this formalism has been considerably expanded, in particular in the analysis of the information transfer between two observational time series (Liang, 2014b, 2015).

The latter approach will be used here to analyze surface mass balance (SMB) changes of the Antarctic ice sheet and to disentangle the rate of information transfer between different observables. SMB over Antarctica is defined as the difference between the snow mass accumulation and the mass loss due to surface sublimation and the sublimation of blowing snow. The net surface meltwater runoff is negligible nearly everywhere over Antarctica in present climate conditions and is generally not included in the Antarctic SMB (Lenaerts et al., 2019).

The climate of the high latitudes of the Southern Hemisphere is characterized by complex interactions between the atmosphere, the ocean, and the ice. Many studies have put forward a strong influence on Antarctica of both tropical and extratropical modes of variability as well as of the changes in sea ice in the Southern Ocean (Ding et al., 2011; Lenaerts et al., 2018; Raphael, 2007; Thomas et al., 2017; Thompson et al., 2011). These studies provide key observables whose influence on SMB can be estimated, and further compared, using classical correlation and the information transfer approach.

In section 2, the methodology is described with a detailed analysis of its ability to characterize the influence of one variable on another in the context of a linear stochastic system. The observables and the data sets that are analyzed are then described in section 3. Section 4 discusses the main results, and conclusions are drawn in section 5.

2. Methodology

Recently, a rigorous formalism of the rate of information transfer between two variables, X_1 and X_2, in deterministic and stochastic dynamical systems has been developed (Liang, 2014a, 2014b, 2015, 2016). This quantity is computed as the difference between the rate of change of the marginal entropy of X_1 and the rate of change of the marginal entropy of X_1 when X_2 is frozen (see Liang, 2014b, together with the Supporting Information S1 in which the key concepts are developed).

These theoretical results were used successfully in the understanding of information transfers between system's variables in various contexts (see, e.g., Liang, 2014a, 2014b). But when dealing with measurement time series, the access to the underlying dynamics is not straightforward due to the complex (linear and nonlinear) interactions between the different elements of the system. To overcome these problems, Liang (2014b) proposes to assume that the underlying dynamics are in a first approximation linear, as often done in data analysis of climate time series (e.g., Sardeshmukh & Sura, 2009). In this case, the rate of information transfer from variable X_2 to X_1, $T_{2\to1}$, can be evaluated in terms of covariances as

$$T_{2\to1} = \frac{C_{11}C_{12}C_{2,d1} - C_{12}^2 C_{1,d1}}{C_{11}^2 C_{22} - C_{11}C_{12}^2}, \tag{1}$$

where $C_{i,j}$ are the usual covariances between variable X_i and X_j and $C_{i,dj}$ are the covariances between the variable X_i and the tendency $\mathrm{d}X_j/\mathrm{d}t$ (evaluated through a Euler forward finite difference). As argued in Liang (2014b), this novel approach offers new insight on the transfer of information between variables much beyond the correlation analysis, even in a nonlinear context, and is easy to implement.

Let us briefly evaluate $T_{i\to j}$ in the context of a stochastic 2-dimensional linear system to clarify the type of information that can be extracted from this, as in Liang (2014b),

$$\begin{aligned} \frac{\mathrm{d}X_1}{\mathrm{d}t} &= a_{1,1}X_1 + a_{1,2}X_2 + \xi_1(t) \\ \frac{\mathrm{d}X_2}{\mathrm{d}t} &= a_{2,2}X_2 + a_{2,1}X_1 + \xi_2(t), \end{aligned} \tag{2}$$

where $\xi_1(t)$ and $\xi_2(t)$ are white noise processes with mean 0 and autocovariance, $< \xi_i(t)\xi_i(t') >= 0.01\delta(t-t')$ for both $i = 1, 2$, where $< . >$ indicates ensemble average. In Figure 1a, $T_{1\to2}$ and $T_{2\to1}$, computed analytically, are represented for arbitrarily chosen parameter values, $a_{1,1} = a_{2,2} = -1$ and $a_{1,2} = 0.5$ as a function of $a_{2,1}$. The correlation is also displayed. First $T_{1\to2}$ and $T_{2\to1}$ are clearly distinct, indicating an asymmetry, contrary to the correlation. When the correlation is equal to 0, both $T_{1\to2}$ and $T_{2\to1}$ are equal to 0. Finally, when $a_{2,1} = 0$, $T_{1\to2} = 0$ but not $T_{2\to1}$ and the correlation. Three typical situations are expected: (i) no correlation and no transfer of information, (ii) correlation but no transfer of information, and (iii) correlation with transfer of information. Note that positive (negative) values of $T_{i\to j}$ mean that the influence of variable i

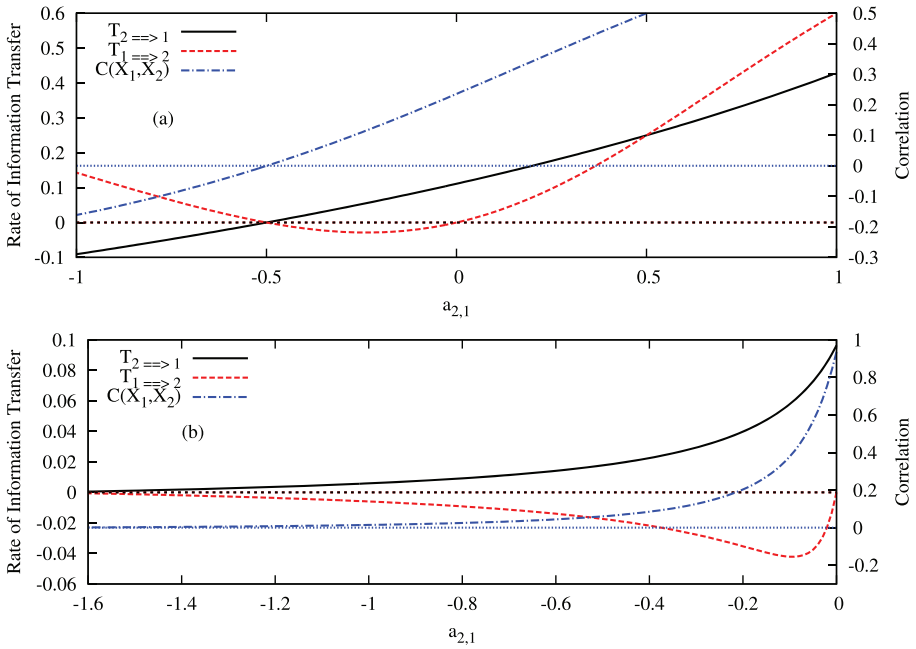

Figure 1. Theoretical values of the rate of information transfer and correlation as a function of the coefficient $a_{2,1}$ of the stochatic linear model described by equation (2). In (a), the other model parameters are fixed to $a_{1,1} = a_{2,2} = -1$ and $a_{1,2} = 0.5$ and, in (b), to $a_{1,1} = -0.1$, $a_{2,2} = -0.01$, $a_{1,2} = 0.17$. The rates of information transfer from 2 to 1 and from 1 to 2 are denoted as "$T_{2\to1}$" and "$T_{1\to2}$" in the legends of each panel. $C(X_1, X_2)$ denotes the correlation between X_1 and X_2.

makes the value of variable j more (less) uncertain or in other words induces a larger (smaller) set of possible outcomes of variable j.

One can also wonder what are the amplitudes of these quantities for which a linear stochastic system is a realistic modeling framework. In recent years, there were convincing evidences that the El Niño-Southern Oscillation can be described by a simple recharge oscillator (Burgers et al., 2005). In this case, typical values of the parameters are $a_{1,1} = -0.1$, $a_{2,2} = -0.01$, $a_{1,2} = 0.17$, and $a_{2,1} = -0.17$. In Figure 1b, $T_{i\to j}$ and correlation are displayed as a function of $a_{2,1}$. When the amplitude of $a_{2,1}$ is small, the correlation is high, and the rates of information transfer have opposite signs. The origin of the increasing correlation for $a_{2,1}$ going to 0 is related to the strong influence of X_2 on X_1, also associated with a larger value of $T_{2\to1}$. At the same time, when $a_{2,1}$ reaches 0, $T_{1\to2}$ also cancels out indicating the decoupling of variable X_2 from X_1.

Let us now turn to the estimation of equation (1) on finite time series. The estimates are represented in Figures 2a and 2b for a series sampled every 0.1 time units. The error bar is obtained by a bootstrapping method with replacement, assuming Gaussian statistics. As the number of records, L, increases, the rate of information transfer converges toward their analytical value. The slight discrepancy for $T_{2\to1}$ is attributed to the discretization of the derivative with the sampling time used. For smaller sampling times, the estimation is closer to the theoretical value. Note that although correlation becomes significant (different from 0) once the length of the time series is larger than 200, much larger data sets are however needed to get $T_{2\to1}$ significantly different from 0 (Figure 2b).

3. Data Sets

3.1. Defining the Observables

The SMB in Antarctica is influenced by changes in atmospheric circulations as well as by the surface conditions in the Southern Ocean (Lenaerts et al., 2019; Thomas et al., 2017), represented here by the sea ice concentration (SIC).

The atmospheric circulation variability is estimated using three standard indices in order to get a first evaluation of the technique. Many studies have also identified strong covariances between 2-m surface air temperature (SAT) and SMB variations (Frieler et al., 2015; Krinner et al., 2007). This variable is thus included in our analyses. The observables used are

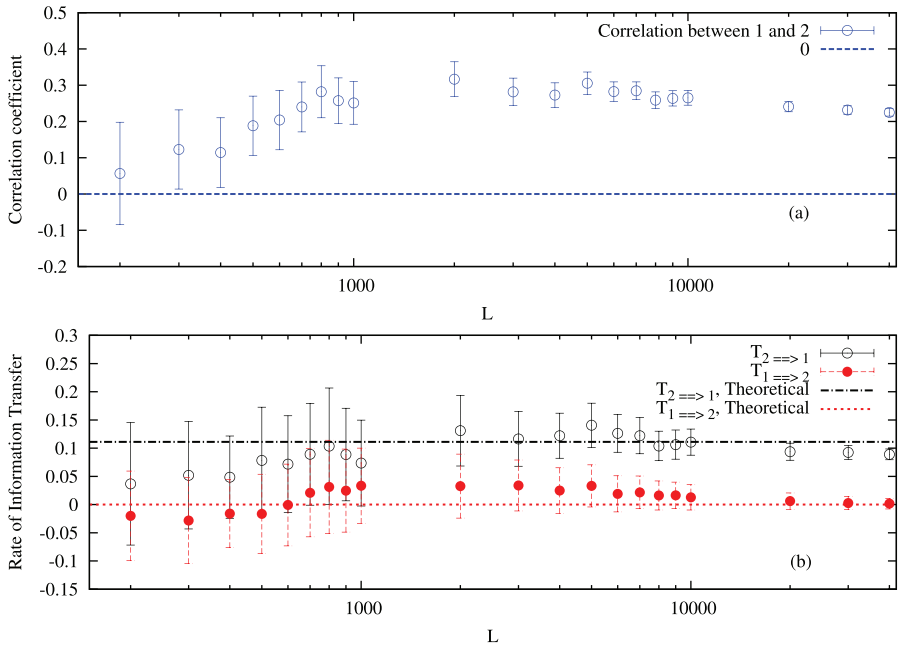

Figure 2. Estimations of the correlation coefficient (a) and the rate of information transfer (b) as a function of L for $a_{1,1} = a_{2,2} = -1$, $a_{1,2} = 0.5$ and $a_{2,1} = 0$. The theoretical values for $T_{2\to1}$ and $T_{1\to2}$ are represented by the horizontal straight lines. The error bar at the 95% level (statistics assumed to be Gaussian) is also represented for each value of L.

1. SMB;
2. 2-m SAT;
3. The mean SIC describing the fraction of ocean area covered by ice;
4. The Southern Annular Mode (SAM), the dominant mode of atmospheric variability in the extratropics of the Southern Hemisphere. It is characterized by an annular structure with synchronous geopotential height anomalies of opposite signs over midlatitudes and Antarctica (Marshall, 2003). Link between SAM and Antarctic climate have been discussed in, for example, Abram et al. (2014) and Medley et al. (2018). In this study, the SAM index is defined as the normalized zonal averaged 500-hPa geopotential heights between 40°S and 65°S.
5. The zonal wave 3 (ZW3) is a dominant pattern of atmospheric variability over the Southern Ocean and Antarctica on time scales ranging from daily to interannual time scales. The ZW3 index is computed as the mean of the normalized 500-hPa geopotential heights at the three ridges that characterize ZW3 (average of grid points from longitudes 45–60°E, 161–171°E, and 71–81°W and latitudes 45–60°S; ; Hobbs & Raphael, 2009; Raphael, 2004).
6. The El Niño-Southern Oscillation. Many studies have demonstrated links between Antarctica and tropical regions (e.g., Clem et al., 2018; Ding et al., 2011; Ionita et al., 2018). Here we use Nino 3.4 sea surface temperature index to represent tropical changes (hereafter El Nino 3.4), defined as sea surface temperature averaged over the region 170–120°W and 5°S–5°N.

3.2. Model Data and Reanalysis

Simulations outputs from the coupled global climate model CESM1-CAM5 (Lehner et al., 2015) and MPI-ESM-P (Stevens et al., 2013) covering the 850–2005 period are analyzed. These simulations are driven by both anthropogenic (greenhouse gases, aerosol, ozone, and land use) and natural (solar, volcanic, and orbital) forcing (Schmidt et al., 2012). They were chosen since they provide very long time series at annual time scale (1,156 years). A brief overview of the quality of their simulated climate is provided in Text S2, see also Dalaiden et al. (2019) and Klein et al. (2019). These models have been chosen because they reproduce reasonably well the mean state and the correlation between SMB and atmospheric circulation.

The ERA-Interim data set (Dee et al., 2011), considered as one of the best reanalysis products for the Antarctic region (e.g., Agosta et al., 2015; Bromwich et al., 2011), reproduces reasonably well the observed state of SMB and SAT (Figure S1) and the atmospheric circulation (Figure S2). It is available from 1979 to 2018

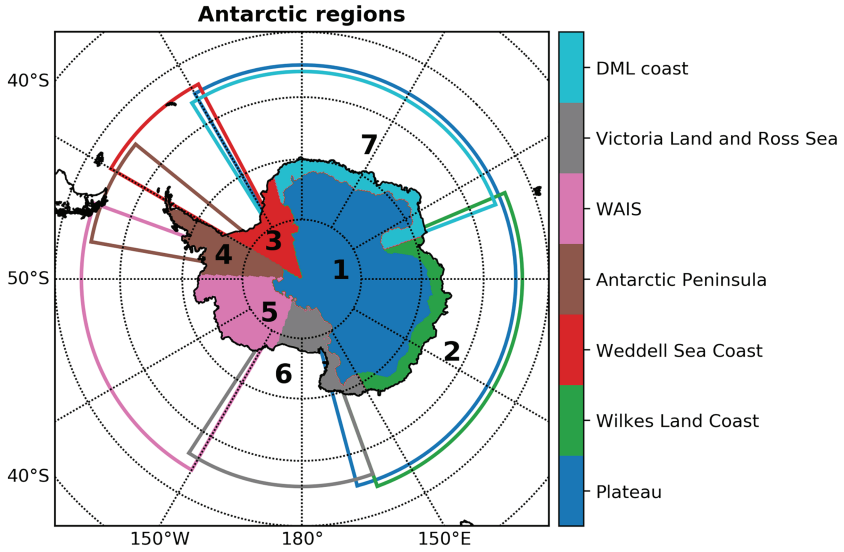

Figure 3. Regional boundaries separating the different regions used in this study. DML = Dronning Maud Land; WAIS = West Antarctica Ice Sheet.

at a spatial resolution of 0.75°. We use the SIC data based on HadISSt and NCEP 2DVAR data before January 2002 (Fiorino, 2004) and on OSTIA afterward (Donlon et al., 2011). These data sets have also been used here, but the length of the reanalysis data set is small (about 40 years), and as alluded in section 2, much longer time series are needed to get rates of information transfer that are significantly different from 0. The results provided as Text S3 suggest that the length of the reanalysis data set does not allow for inferring useful information.

3.3. Defining the Regions

The analyses are performed on SMB averaged over several continental Antarctic regions as in Thomas et al. (2017). East Antarctica above 2,000-m elevation constitutes the Antarctica Plateau (Region 1). The coastal zones are divided into four regions: the Wilkes Land Coast (70–150°E; Region 2), the Weddell Sea Coast (15–60°E; Region 3), the Antarctic Peninsula (Region 4), the West Antarctica Ice Sheet (Region 5), with a division at 88°W, the Victoria Land and Ross Sea (150–170°E; Region 6) and the Dronning Maud Land coast (DML coast; 15°W–150°E; Region 7). These boundaries are also used in computing regional mean SAT. For SIC, an oceanic region is assigned to each of the seven continental regions, following its longitudinal extent: 30°W–165°E, 67–160°E, 60–30°W, 80–50°W, 150–70°W, 150°E–150°W, and 30°W–70°E, respectively, for Regions 1 to 7 (Figure 3).

4. Results

Figures 4 and 5 display the rate of information transfer, $T_{X_1 \to X_2}$, from a set of observables to the SMB over Antarctica, the El Niño, the SAM, and ZW3 indices, together with the corresponding correlations, for two historical simulations with the MPI-ESM-P and CESM1-CAM5 climate models from 850 to 2005. The error bars represent the uncertainty at the 95% level. The observable experiencing the influence of the others is referred as *the Target* in each panel. A first general remark is that many of the observables used display significant correlations with each other, but several of them are not associated with detectable dynamical influences as measured by $T_{X_1 \to X_2}$.

Let us now focus on specific interesting cases related to the influence of the large-scale dynamical modes, SIC, and SAT on SMB. The term influence is used when discussing the results based on $T_{X_1 \to X_2}$, but when needed, the correlation is also explicitly mentioned. We consider that significant influence is present when the error bar at the 95% level does not cross the zero line and vice versa. Results for Regions 1 to 7 of Figure 3 are shown in panels (a) to (g). Additional results are also displayed in Text S4.

4.1. Large-Scale Modes

For the MPI-ESM-P model (Figure 4), El Niño 3.4 is significantly influencing regional SMB over Regions 2 and 3 that are on opposite sides (East and West) of Antarctica, SAM is influencing Regions 4 and 6, and ZW3,

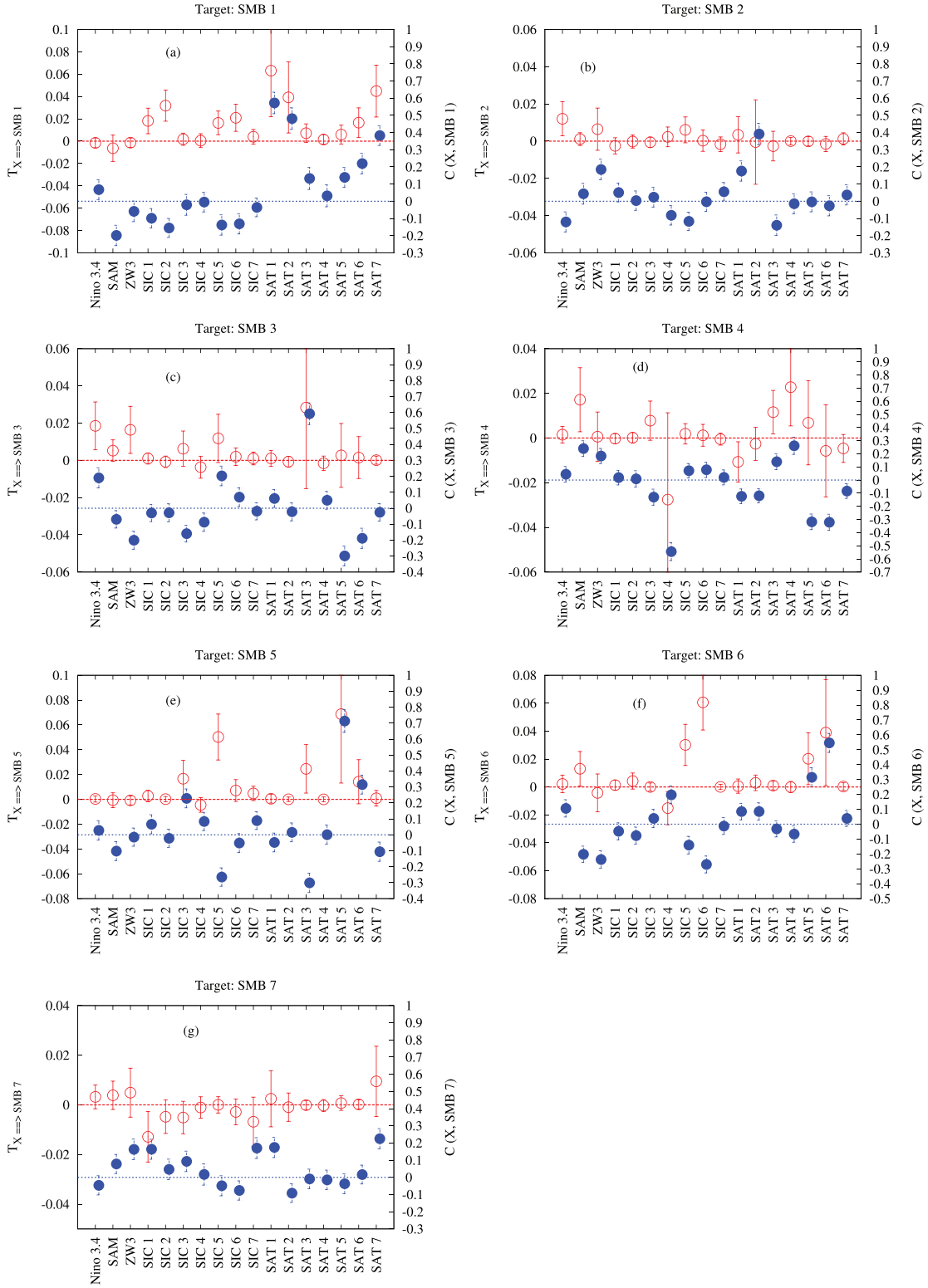

Figure 4. The rate of information transfer and the correlation are plotted as a function of the observables for seven different targeted observables. In (a)–(g), the targeted observable is referred to as the "Target" in the title, and the rate of information transfer from the other observables is plotted in red with the scale on the left vertical axis. The corresponding correlation coefficient is plotted in blue with the scale on the right vertical axis. The data used are coming from one specific run (Run 1) from an ensemble of runs made with the MPI-ESM-P climate model from 850 to 2005. Along the horizontal axis, the different observables used are the sea surface temperature of Nino 3.4 region, the Southern Annular Mode (SAM) index, the zonal wave 3 (ZW3) mode over Antarctica, the sea ice concentration (SIC), and the 2-m surface air temperature (SAT) averaged over the seven regions (Regions 1–7). SMB = surface mass balance.

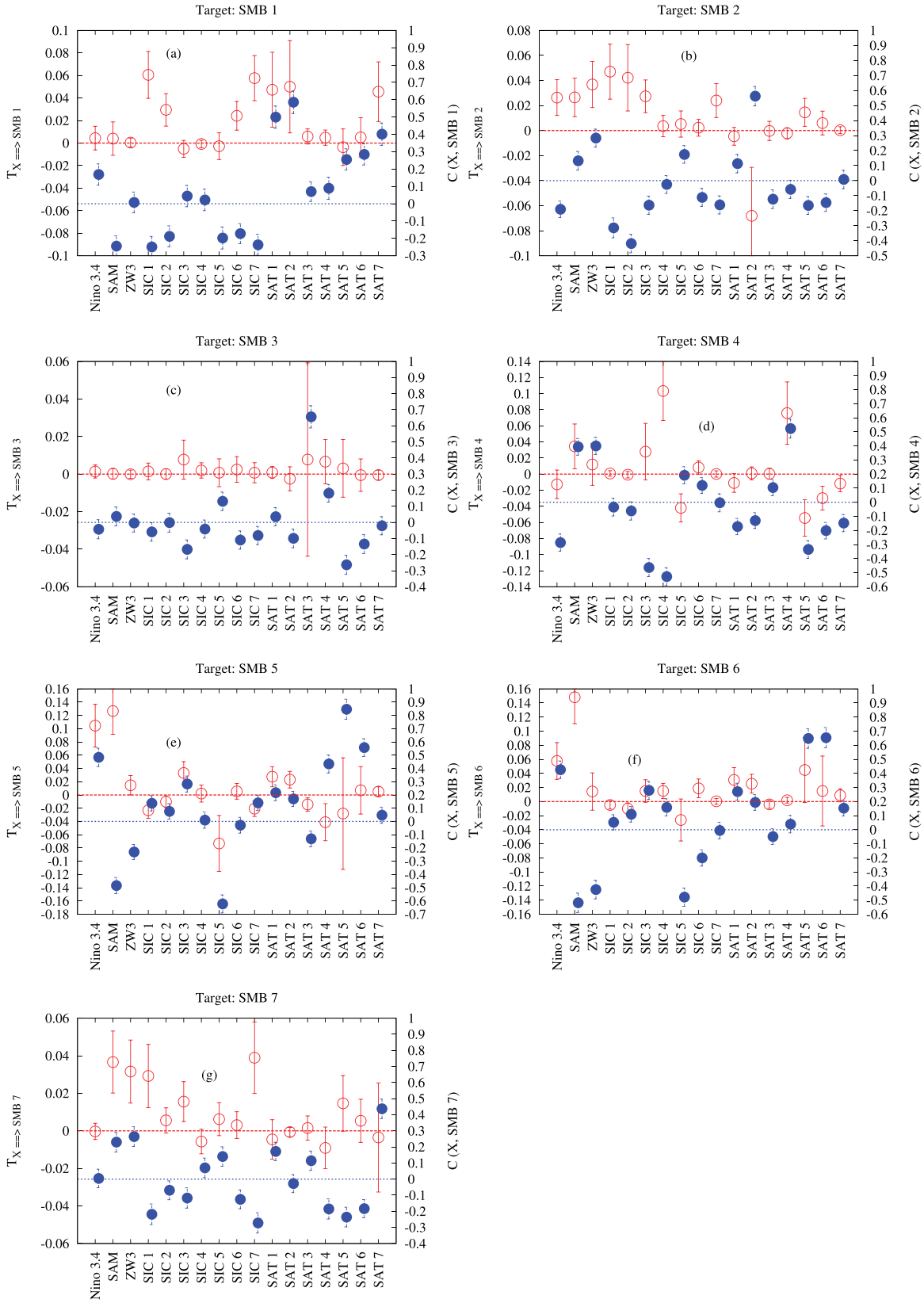

Figure 5. As in Figure 4 for the CESM1-CAM5 model. The run used here is Run 10 of the ensemble produced with the CESM1-CAM5 model from 850 to 2005.

Region 3 only. Interestingly, several highly significant correlations of ZW3 with the SMB over Regions 2, 4, 6, and 7 do not lead to any dynamical dependence. It indicates that previous links expected from the computations of correlations between large-scale modes and observables over Antarctica are not necessarily of dynamical origine but rather a covariability whose origin should be found in the common influence of upstream processes.

For CESM1-CAM5 (Figure 5), the picture is slightly different, with El Niño 3.4 significantly influencing Regions 2, 5, and 6, SAM influencing Regions 2, 4, 5, 6, and 7, and ZW3 influencing Regions 2 and 7. This model overall displays a stronger influence of the climate modes on the SMB than the MPI-ESM-P model. CESM1-CAM5 has stronger correlation between SMB and geopotential height than MPI-ESM-P (Figure S2) but also than ERA-Interim, suggesting that it may also overestimate the influence of circulation modes on SMB.

Interestingly, none of them are showing any influence on the Plateau (Region 1) although important significant correlations are found with El Niño and SAM.

In both models, the influence of SAM on the Antarctic Peninsula and the Victoria Land and Ross Sea is marked. SAM is also expected to have an influence on many other coastal regions (e.g., Medley et al., 2018). This can be masked for some regions by the specific box averaging, as, for instance, for West Antarctica Ice Sheet (Region 5) for MPI-ESM-P where SAM can induce positive and negative SMB anomaly inside the box. El Nino 3.4 is also expected to have an influence on many regions (e.g., Clem et al., 2018; Kohyama & Hartmann, 2017) in particular on West Antarctica, but it is detected here only in CESM1-CAM5 and in the Indian Sector, which may be related to the influence over Wilkes Land in both models.

Several studies have suggested decreased precipitation over the Antarctic Plateau associated to a positive SAM index (e.g., Marshall et al., 2017; Medley et al., 2018), in agreement with the significant correlation found for both models (Figures 4 and 5). Nevertheless, the absence of dependence indicates that the link is not of dynamical nature. Rather, the changes should be associated with local thermodynamic processes in Region 1 as discussed below. If SAM has an influence at all, it would probably be associated with modifications of temperature conditions.

4.2. SIC

For the MPI-ESM-P model (Figure 4), SIC of Regions 1, 2, 5, and 6 are influencing the SMB over Region 1, SIC of Region 5 is influencing SMB of Region 5, and SIC of Regions 4–6 are influencing the SMB of Region 6. Here also some high and significant correlations do not lead to significant dependence like for the influence of SIC on SMB of Region 4.

For the CESM1-CAM5 model (Figure 5), SIC of Regions 1, 2, 5, and 6 are again influencing the SMB over Region 1, but now SIC over Region 7 is also influencing SMB over Region 1. Contrary to the MPI-ESM-P model, the SMB over Region 2 is here influenced by the SIC over Regions 1, 2, 3, and 7. The SMB over Region 4 is influenced by SIC over Regions 4 and 5, result also different to the ones obtained with the MPI-ESM-P model. The SMB over Region 5 is influenced by SIC over Regions 1, 2, 3, 5, and 7, over Region 6, by SIC of Regions 4 and 6, and over Region 7, by SIC of Regions 1, 3, and 7.

Remarkably, the SMB in Region 3 (Weddell sea coast) is not influenced by SIC in any model despite significant correlations.

Finally, as for the large-scale modes, the CESM1-CAM5 model displays in general stronger influences of SIC over the SMB of Antarctica that could be related to a larger mean sea ice extent and thus larger amplitude variations in SIC than in MPI-ESM-P.

4.3. SAT

For the MPI-ESM-P model (Figure 4), SATs of Regions 1, 2, 6, and 7 are influencing the SMB over Region 1. SMB of Region 4 is influenced by SATs of Regions 3 and 4; SMB of Region 5 by the SATs of Regions 3 and 5; and SMB of Region 6 by SATs of Regions 5 and 6.

For the CESM1-CAM5 model (Figure 5), SATs of Regions 1, 2, 3, and 7 are again influencing the SMB over Region 1. SMB of Region 2 is now influenced by the SATs of Regions 2 and 5; SMB of Region 4 by SAT in Regions 4–7; and SMB of Region 6 by SAT of Regions 1, 2, and 7.

A dependence of SMB on temperature and mean SIC is expected from basic thermodynamic processes. Less sea ice induces more evaporation from the open ocean surface and then potentially more precipitation, while temperature influences the moisture content through the Clausius-Clapeyron law (Altnau et al., 2015; Frieler et al., 2015; Monaghan et al., 2008). This link appears stronger inside the continent than on the coast as clear dependence is found in both models for temperature and SIC for the Antarctic Plateau (Region 1, Figures 4a and 4b). This region is the largest one including zones further away from the coast, where it is expected that a robust thermodynamic link is present. By contrast, SMB over the Weddell Sea Coast and DML coast are not influenced by SAT in both model runs. These two regions have potentially larger influence of air masses coming from the ocean and display strong topographic gradients. This can impose a strong signature of multiple regional processes with a complex interplay between circulation, temperature, and precipitation (Lenaerts et al., 2013, 2019; Turner et al., 2019).

5. Conclusions

The analysis of the influence of certain processes on others in climate science is often based on correlation. Although the statistics based on this quantity are useful to have a first clue on the presence of a link between two observables, it cannot be used to infer any dynamical influence between them. Recent developments on information transfer in dynamical systems provide new tools to investigate dynamical interactions (Liang, 2014b). The power of the approach has been successfully demonstrated here by the use of a simple measure of directional dynamical influence between observables in the context of the analysis of the link between the SMB over Antarctica and a set of other surface observables and global indices.

As measurement data are sparse and do not cover a long period, the analysis has been performed in the context of two long climate simulations on a yearly basis, obtained with the MPI-ESM-P and CESM1-CAM5 climate models, known to provide good representations of the Antarctic climate as discussed in the supporting information. Although dynamical connections between SMB and the other observables are stronger in the CESM1-CAM5 model than in MPI-ESM-P, a few key results concerning the dependence of SMB, coherent between the two models, are emerging: (i) The Antarctic Plateau is not influenced by the large-scale modes but well by the SAT and SIC; (ii) the SMB over the Weddell Sea coast and the DML coast are not influenced by the SAT; and (iii) the Weddell Sea coast is not dynamically influenced by the SIC.

Acknowledgments
This work is supported in part by the project Mass2Ant (BR/165/A2/Mass2Ant) of the Belgian Science Policy Office. H. Goosse is Research Director within the F.R.S.-FNRS, Belgium. The data sets used in the present paper are coming from main data sources websites: All CMIP5/PMIP3 model simultation including the MPI-ESM-P simulation are available online (https://pcmdi9.llnl.gov); the CESM1-CAM5 ensemble over the last millenium can be directly downloaded online (https://www.earthsystemgrid.org); the ERA-interim reanalysis is available from the ECMWF website (https://www.ecmwf.int/en/research/climate-reanalysis/era-interim).

References

Abarbanel, H. D. I., Masuda, N., Rabinovitch, M. I., & Turner, E. (2001). Distribution of mutual information. *Physics Letters A*, *281*, 368–373.
Abram, N., Mulvaney, R., Vimeux, F., Phipps, S., & Turner, J. (2014). Evolution of the Southern Annular Mode during the past millennium. *Nature Climate Change*, *4*, 564–569.
Agosta, C., Fettweis, X., & Datta, R. (2015). Evaluation of the CMIP5 models in the aim of regional modelling of the Antarctic surface mass balance. *Cryosphere*, *9*, 3113–3136.
Alexander, M. A., Bladé, I., Newman, M., Lanzante, J. R., Lau, N.-C., & Scott, J. D. (2002). The atmospheric bridge: The influence of ENSO teleconnections on air-sea interaction over the global oceans. *Journal Climate*, *15*, 2205–2231.
Altnau, S., Schlosser, E., Isaksson, E., & Divine, D. (2015). Climatic signals from 76 shallow firn cores in Dronning Maud Land, East Antarctica. *Cryosphere*, *9*(3), 925–944.
Bianco-Martinez, E., & Baptista, M. S. (2018). Space-time nature of causality. *Chaos*, *28*, 75509.
Bromwich, D., Nicolas, J., & Monaghan, A. (2011). An assessment of precipitation changes over Antarctica and the Southern Ocean since 1989 in contemporary global reanalyses. *Journal Climate*, *24*, 4189–4209.
Brönnimann, S. (2007). Impact of El-Niño-Southern Oscillation on European climate. *Reviews of Geophysics*, *45*, RG3003. https://doi.org/10.1029/2006RG000199
Burgers, G., Jin, F-F., & van Oldenborgh, G. J. (2005). The simplest ENSO recharge oscillator. *Geophysical Research Letters*, *32*, L13706. https://doi.org/10.1029/2005GL022951
Clem, K., Renwick, J., & Mcgregor, J. (2018). Autumn cooling of Western East Antarctica linked to the tropical Pacific. *Journal of Geophysical Research: Atmospheres*, *123*, 89–107. https://doi.org/10.1002/2017JD027435
Dalaiden, Q., Goosse, H., Klein, F., Lenaerts, J., & Holloway, M. (2019). Surface mass balance of the Antarctic Ice Sheet and its link with the Antarctic climate through global coupled model simulations and reconstructions. *The Cryosphere Discuss*. https://doi.org/10.5194/tc-2019-111, in review.
Dee, D., et al. (2011). The ERA-interim reanalysis: Configuration and performance of the data assimilation system. *Quarterly Journal of the Royal Meteorological Society*, *137*, 553–597.
Deza, J., Barreiro, M., & Masoller, C. (2015). Assessing the direction of climate interactions by means of complex networks and information theoretic tools. *Chaos*, *25*, 33105.
Ding, Q., Steig, E., Battisti, D., & Küttel, M. (2011). Winter warming in West Antarctica caused by central tropical Pacific warming. *Nature Geoscience*, *4*, 398–403.
Donlon, C., Martin, M., Stark, J., Roberts-jones, J., Fiedler, E., & Wimmer, W. (2011). The Operational Sea Surface Temperature and Sea Ice Analysis (OSTIA) system. *Remote Sensing of Environment*, *116*, 140–158.

Fiorino, M. (2004). A multi-decadal daily sea surface temperature and sea ice concentration data set for the ERA-40 reanalysis (*ERA-40 Project Report Series, No 12*): ECMWF, 16.
Frieler, K., Clark, P., He, F., Buizert, C., Reese, R., Ligtenberg, S., et al. (2015). Consistent evidence of increasing Antarctic accumulation with warming. *Nature Climate Change*, *5*, 348–352.
Hlavackova-Schindler, M., Palus, M., Vejmelka, M., & Bhattacharya, J. (2007). Causality detection based on information-theoretic approaches in time series analysis. *Physics Report*, *441*, 1–46.
Hobbs, W. R., & Raphael, M. N. (2009). Characterizing the zonally asymmetric component of the SH circulation. *Climate Dynamics*, *35*, 859–873.
Ionita, M., Scholz, P., Grosfeld, K., & Treffeisen, R. (2018). Moisture transport and Antarctic sea ice: Austral spring 2016 event. *Earth System Dynamics*, *9*, 939–954.
Klein, F., Abram, N. J., Curran, M. A. J., Goosse, H., Goursaud, S., Masson-Delmotte, V., et al. (2019). Assessing the robustness of Antarctic temperature reconstructions over the past two millennia using pseudoproxy and data assimilation experiments. *Climate of the Past*, *15*, 661–684.
Kohyama, T., & Hartmann, D. L. (2017). Nonlinear ENSO warming suppression (NEWS). *Journal Climate*, *30*, 4227–4251.
Krakovská, A., Jakubík, J., Chvosteková, M., Coufal, D., Jackay, N., & Palus, M. (2018). Comparison of six methods for the detection of causality in a bivariate time series. *Physical Review E*, *97*, 42207.
Krinner, G., Simmonds, I., Genthon, C., & Dufresne, J. (2007). Simulated Antarctic precipitation and surface mass balance of the end of the 20th and 21st centuries to cite this version: HAL Id: Hal-00184741 Simulated Antarctic precipitation and surface mass balance at. *Climate Dynamics*, *28*, 215–230.
Lau, N.-C. (2016). 2015 Bernhard Haurwitz Memorial Lecture: Model diagnosis of El-Niño teleconnections to the global atmosphere-ocean system. *Bulletin of the American Meteorological Society*, *97*, 981–988.
Lehner, F., Joos, F., Raible, C., Mignot, J., Born, A., Kelle, K., & Stocker, T. (2015). Climate and carbon cycle dynamics in a CESM simulation from 850 to 2100 CE. *Earth System Dynamics*, *6*, 411–434.
Lenaerts, J., Fyke, J., & Medley, B. (2018). The signature of ozone depletion in recent Antarctic precipitation change: A study with the Community Earth System Model. *Geophysical Research Letters*, *45*, 12,931–12,939. https://doi.org/10.1029/2018GL078608
Lenaerts, J. T. M., Medley, B., van den Broecke, M. R., & Wouters, B. (2019). Observing and modeling ice sheet surface mass balance. *Reviews in Geophysics*, *57*, 376–420. https://doi.org/10.1029/2018RG000622
Lenaerts, J. T., Van Meijgaard, E., Van Den Broeke, M. R., Ligtenberg, S. R., Horwath, M., & Isaksson, E. (2013). Recent snowfall anomalies in Dronning Maud Land, East Antarctica in a historical and future climate perspective. *Geophysical Research Letters*, *40*, 2684–2688. https://doi.org/10.1002/grl.50559
Liang, X. S. (2008). Information flow within stochastic dynamical systems. *Physical Review E*, *78*, 31113.
Liang, X. S. (2014a). Entropy evolution and uncertainty estimation with dynamical system. *Entropy*, *16*, 3605–3634.
Liang, X. S. (2014b). Unraveling the cause-effect relation between time series. *Physical Review E*, *90*, 52150.
Liang, X. S. (2015). Normalizing the causality between time series. *Physical Review E*, *92*, 22126.
Liang, X. S. (2016). Information flow and causality as rigorous notions ab initio. *Physical Review E*, *94*, 52201.
Liang, X. S., & Kleeman, R. (2005). Information transfer between dynamical system components. *Physical Review E*, *95*, 244101.
Liang, X. S., & Kleeman, R. (2007). A rigourous formalism of information transfer between dynamical system components, II. Continuous flow. *Physica D*, *227*, 173–182.
Luo, M., Kantz, H., Lau, N.-C., Huang, W., & Zhou, Y. (2015). Questionable dymamical evidence for causality between galactic cosmic rays and interannual variation in global temperature. *PNAS*, *112*, E4,638–E4,639.
Ma, H., Leng, S., & Chen, L. (2018). Data-based prediction and causality inference of nonlinear dynamics. *Science China Mathematics*, *61*, 403–420.
Marshall, G. (2003). Trends in the Southern Annular Mode from observations and reanalyses. *Journal Climate*, *16*, 4134–4143.
Marshall, G. J., Thompson, D. W., & van den Broeke, M. R. (2017). The signature of Southern Hemisphere atmospheric circulation patterns in Antarctic precipitation. *Geophysical Research Letters*, *44*, 11,580–11,589. https://doi.org/10.1002/2017GL075998
Medley, B., Mcconnell, J., Neumann, T., Reijmer, C., Chellman, N., Sigl, M., & Kipfstuhl, S. (2018). Temperature and snowfall in western Queen Maud Land increasing faster than climate model projections. *Geophysical Research Letters*, *45*, 1472–1480. https://doi.org/10.1002/2017GL075992
Monaghan, A. J., Bromwich, D. H., & Schneider, D. P. (2008). Twentieth century Antarctic air temperature and snowfall simulations by IPCC climate models. *Geophysical Research Letters*, *35*, L07502. https://doi.org/10.1029/2007GL032630
Raphael, M. (2004). A zonal wave 3 index for the Southern Hemisphere. *Geophysical Research Letters*, *31*, L23212. https://doi.org/10.1029/2004GL020365
Raphael, M. (2007). The influence of atmospheric zonal wave three on Antarctic sea ice variability. *Journal of Geophysical Research*, *112*, D12112. https://doi.org/10.1029/2006JD007852
Runge, J., Heitzig, J., Marwan, N., & Kurths, J. (2012). Quantifying causal coupling strength: A lag-specific measure for multivariate time series related to tranfer entropy. *Physical Review E*, *86*, 61121.
Sardeshmukh, P. D., & Sura, P. (2009). Reconciling non-Gaussian climate statistics with linear dynamics. *Journal Climate*, *22*, 1193–1207.
Schmidt, G., et al. (2012). Climate forcing reconstructions for use in PMIP simulations of the Last Millennium (v1.1). *Geoscientific Model Development*, *5*, 185–191.
Schreiber, T. (2000). Measuring information transfer. *Physical Review Letters*, *85*, 461.
Shannon, C. E. (1948). A mathematical theory of communication. *Bell System Technical Journal*, *27*, 379–423.
Stevens, B., Giorgetta, M., Esch, M., Mauritsen, T., Crueger, T., Rast, S., et al. (2013). Atmospheric component of the MPI-M Earth system model: ECHAM6. *Journal Of Advances In Modeling Earth Systems*, *5*, 146–172. https://doi.org/10.1002/jame.20015
Sugihara, G., May, R., Ye, H., Hsieh, C.-H., Deyle, E., Fogarty, M., & Munch, S. (2012). Detecting causality in complex ecosystems. *Science*, *338*, 496–500.
Thomas, E., van Wessem, J. M., Roberts, J., Isaksson, E., Schlosser, E., Fudge, T. J., et al. (2017). Regional Antarctic snow accumulation over the past 1000 years. *Climate Of The Past*, *13*, 1491–1513.
Thompson, D., Solomon, S., Kushner, P., Grise, K., & Karoly, D. (2011). Signatures of the Antarctic ozone hole in Southern Hemisphere surface climate change. *Nature Geoscience*, *4*, 741–749.
Tsonis, A. A., Deyle, E., May, R., Sugihara, G., Swanson, K., Verbeten, J., & Wang, G. (2015). Dynamical evidence for causality between galactic cosmic rays and interannual variation in global temperature. *PNAS*, *112*, 3253–3256.
Turner, J., Phillips, T., Thamban, M., Rahaman, W., Marshall, G. J., Wille, J. D., et al. (2019). The dominant role of extreme precipitation events in Antarctic snowfall variability. *Geophysical Research Letters*, *46*, 3502–3511. https://doi.org/10.1029/2018GL081517

Vannitsem, S., & Ekelmans, P. (2018). Causal dependences between the coupled ocean-atmosphere dynamics over the tropical Pacific, the North Pacific and the North Atlantic. *Earth System Dynamics*, *9*, 1063–1083.

Vannitsem, S., & Ghil, M. (2017). Evidence of coupling in ocean-atmosphere dynamics over the North Atlantic. *Geophysical Research Letters*, *44*, 2016–2026. https://doi.org/10.1002/2016GL072229

Vastano, J. A., & Swinney, H. L. (1988). Information transport in spatiotemporal systems. *Physical Review Letters*, *60*, 1773–1776.

Ye, H., Sugihara, G., Deyle, E. D., May, R. M., Swanson, K., & Tsonis, A. A. (2015). Reply to Luo others: Robustness of causal effects of galactic cosmic rays on interannual variation in global temperature. *PNAS*, *112*, E4,640–E4,641.